Multidisciplinary
SCIENTIFIC JOURNAL
OF MARITIME RESEARCH

University of Rijeka
FACULTY OF MARITIME STUDIES

Multidisciplinarni
znanstveni časopis
POMORSTVO

https://doi.org/10.31217/p.33.2.8

Multilayer Perceptron approach to Condition-Based Maintenance of Marine CODLAG Propulsion System Components

Ivan Lorencin, Nikola Anđelić, Vedran Mrzljak, Zlatan Car

Faculty of Engineering, University of Rijeka, Vukovarska 58, 51000 Rijeka, Croatia, e-mail: ilorencin@riteh.hr; nandelic@riteh.hr; vedran.mrzljak@riteh.hr; zlatan.car@riteh.hr

ABSTRACT

In this paper multilayer perceptron (MLP) approach to condition-based maintenance of combined diesel-electric and gas (CODLAG) marine propulsion system is presented. By using data available in UCI, online machine learning repository, MLPs for prediction of gas turbine (GT) and GT compressor decay state coefficients are designed. Aforementioned MLPs are trained and tested by using 11 934 samples, of which 9 548 samples are used for training and 2 386 samples are used testing. In the case of GT decay state coefficient prediction, the lowest mean relative error of 0.622 % is achieved if MLP with one hidden layer of 50 artificial neurons (AN) designed with Tanh activation function is utilized. This configuration achieves the best results if it is trained by using L-BFGS solver. In the case of GT compressor decay state coefficient, the best results are achieved if MLP is designed with four hidden layers of 100, 50, 50 and 20 ANs, respectively. This configuration is designed by using Logistic sigmoid activation function. The lowest mean relative error of 1.094 % is achieved if MLP is trained by using L-BFGS solver.

ARTICLE INFO

Original scientific paper
Received 3 October 2019
Accepted 22 October 2019

Key words:
Artificial intelligence
CODLAG Propulsion System Components
Condition-Based Maintenance
Multilayer Perceptron

1 Introduction

With the ever-rising trend of computer utilization in complex engineering problems solving, a possibility of implementing computer technology for solving maintenance problems arises. Maintenance can be defined as a set of operations performed with aim to restore the functionality of an item [1], and it can be divided into two basic types

- Corrective maintenance and
- Preventive maintenance.

Corrective maintenance is a failure-driven maintenance, and it is performed in cases when the item is showing signs of malfunctioning [2]. In other words, corrective maintenance is maintenance performed on principle "fix it when it brakes". Such approach can often produce high maintenance costs due to equipment price, ship delay, etc [3]. On the other hand, preventive maintenance can provide in-time action from the maintenance aspect and can significantly reduce maintenance costs [4]. One approach to preventive maintenance is to perform condition-based maintenance. Condition-based maintenance is maintenance approach that makes decision according to monitored parameters of the process or the object [5]. Decision is often performed by using artificial intelligence (AI) algorithms [6–8]. Condition-based (preventive) maintenance can be also successfully used in marine propulsion systems or its components.

Marine propulsion systems in worldwide fleet nowadays are primarily based on diesel engines of any type [9,10]. The dominant presence of diesel engines enables the development of different numerical models for research and analysis of their operating parameters [11], for optimization of their processes [12] and for investigation of reducing its emissions [13,14].

In some parts of shipping transport industry, the steam propulsion systems have still maintained a dominant role, as in a transport of liquefied natural gas (LNG) [15,16]. The basic elements of such propulsion systems are steam turbines – main [17] and auxiliary [18] along with all of its components necessary for operation [19]. However, the

volume of diesel engines utilization in this part of shipping transport industry is rapidly increasing, due to utilization of dual fuel diesel engines [20].

Along with mentioned ones, it should be noted that new marine propulsion systems which are based on various combinations of gas turbine, steam turbine and diesel engine (or more of them) are currently under the development [21,22]. Such complex systems integrate in one engine room several benefits of each propulsion element in a current combination. Usually, one of many goals in front of such complex marine propulsion systems is reducing overall emissions from the ship [23]. One of such new complex marine propulsion systems is combined diesel-electric and gas (CODLAG) in which electrical motor (driven by diesel-generator) and gas turbine (or more of them) simultaneously drive main propulsion propeller.

In this paper, a multilayer perceptron (MLP) approach for condition-based maintenance of marine CODLAG propulsion system vital parts – gas turbine (GT) and GT compressor is proposed. MLP is a subclass of artificial neural networks (ANN), based on feedforward architecture [24]. Artificial neural networks are today widely used for solving classification and regression tasks in cancer recognition [25, 26], sepsis prediction [27], recognition of marine objects [28], prediction of marine diesel engine parameters [29], etc. MLP can be considered as the most popular ANN subclass, due to its high classification [30,31] and regression performances [32,33] in problems similar to condition-based maintenance of marine CODLAG propulsion system components.

In this research, a possibility of MLP implementation in tasks of GT and GT compressor decay state coefficients prediction is investigated. From these reasons following questions arises:

- Is there a possibility of MLP implementation for GT and GT compressor decay state coefficients prediction?
- How various hyperparameters affect MLP predictive performance?
- How solver type influences MLP predictive performance?

2 Materials and methods

2.1 Dataset description

In this paper, dataset in regard of combined diesel-electric and gas (CODLAG) marine propulsion system which operates in Frigate propulsion plant is used. This dataset is created by using simulation data presented in [6]. On the scheme of CODLAG propulsion system can be seen that propulsion is achieved with combination of electrical motors and GT, Fig. 1.

Electrical power for the operation of electric motors is produced with diesel engine-powered electrical generators (diesel-generators). Power generated with GT and two electrical motors is used to drive two Frigate propellers and it is transmitted through the system designed with three gear boxes and four clutches.

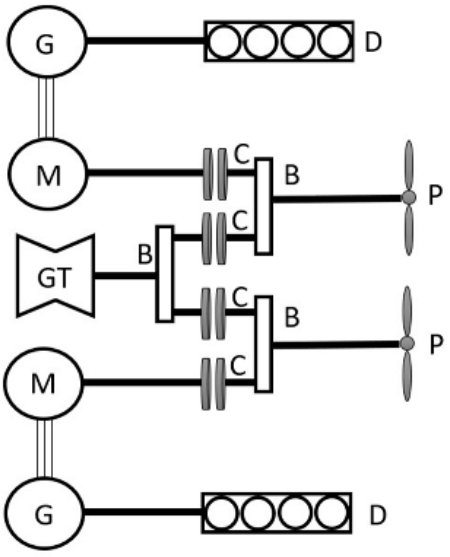

Fig. 1 Scheme of Frigate CODLAG propulsion system (GT – gas turbine; M – electrical motor; G – electrical generator; D – diesel engine; B – gear box; C – clutch; P – Frigate propeller

Source: Authors

GT used in CODLAG propulsion system shown in Fig. 1 is based on two-shaft arrangement with a compressor, high pressure (HP) and low pressure (LP) GT, as presented in Fig. 2. It can be noticed that power produced with HP GT is used for compressor drive only, while power produced with LP GT is used for ship propulsion, together with power produced by electrical motors. In this configuration, HP GT (along with compressor and combustion chamber) is "gas generator" [34] and LP GT is free power shaft turbine, without any mechanical connection to HP GT (connection is achieved only by the flue gases).

The decay state coefficient can be used as a numerical indicator of the GT and GT compressor condition and it can be used as an indicator of system maintenance needs. Decay of GT and GT compressor is simulated in [6] using MatLab where is concluded that decay of GT and GT compressor is the consequence of fouling. Source of fouling can be found in exhaust gases and oil vapors that produce a layer of impurities on the blades of GT and in impurities of air which enters in GT compressor suction side (regardless of air filter usage). The simulation effect of fouling is, in the case of GT compressor, simulated as a decrease of airflow rate M_c and isentropic efficiency η_c. In the case of GT, fouling is simulated as gas flow rate decrease.

Dataset described in [6] is publicly available in UCI online machine learning repository and it consists of 16 input parameters and two output parameters, shown in Table 1. It should be noted that in decay state coefficients analysis, from this point on, term gas turbine (GT) is related to both turbine cylinders (HP and LP).

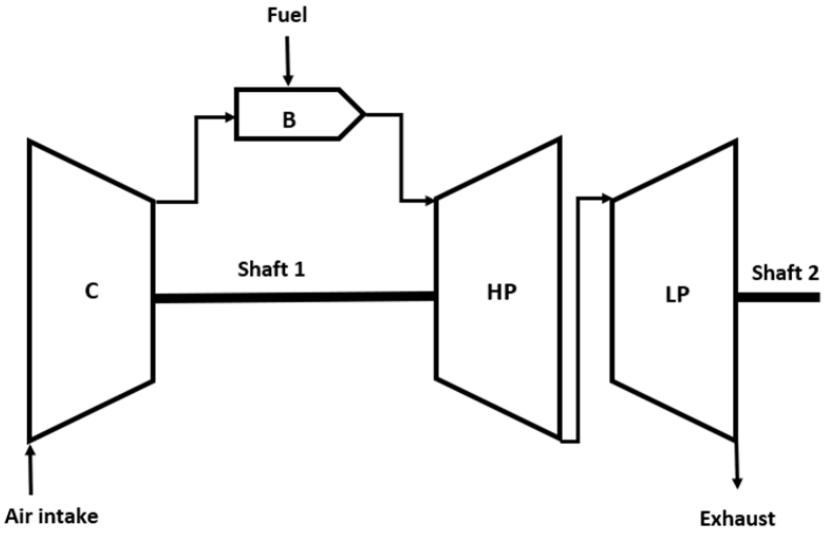

Fig. 2 Scheme of gas turbine used in marine CODLAG propulsion system
(C – compressor; B – combustion chamber; HP – high pressure turbine; LP – low pressure turbine)

Source: Authors

Table 1 Dataset parameters

Input parameters		
Parameter	**Range**	**Unit**
Lever position	1.138 – 9.3	-
Ship speed (v)	3 – 27	kn
LP turbine shaft torque (LPT)	253.547 – 72784.872	kNm
LP turbine rate of revolutions (LPn)	1307.675 – 3560.741	rpm
Gas generator rate of revolutions (GGn)	6589.002 – 9797.103	rpm
Starboard propeller torque (Ts)	5.304 – 645.249	kNm
Port propeller torque (Tp)	5.304 – 645.249	kNm
HP turbine exit temperature (T48)	442.364 – 1115.797	K
GT compressor inlet air temperature (T1)	288	K
GT compressor outlet air temperature (T2)	540.442 – 789.094	K
HP turbine exit pressure (P48)	1.093 – 4.56	bar
GT compressor inlet air pressure (P1)	0.998	bar
GT compressor outlet air pressure (P2)	5.828 – 23.14	bar
LP turbine exit pressure (Pexh)	1.019 – 1.052	bar
Combustion chamber injection control (CCIC)	0 – 92.556	%
Fuel flow (mf)	0.068 – 1.832	kg/s
Output parameters		
GT compressor decay state coefficient	0.95 – 1	-
GT decay state coefficient	0.975 – 1	-

Dataset consists of 11 934 samples in total, of which 9 548 samples are used for MLP regressor training and 2 386 samples are used for MLP regressor testing.

Source: Authors

2.2 Multilayer perceptron (MLP)

For the purpose of this research, MLP is used. MLP is a type of feed-forward artificial neural network (ANN) which is characterized with three different layer types:

- input layer,
- hidden layer and
- output layer.

If MLP is well designed, it can distinguish data that is not linearly separable. Because of this property, MLP can be utilized for solving various regression and classification

problems [35]. Every artificial neuron (AN), the key building element of each MLP, is designed by using activation function [36]. Output of each AN is defined by activation function (Y):

$$\boldsymbol{Y} = \boldsymbol{f}(\boldsymbol{u}), \tag{1}$$

where u represents a sum of all AN weights (w_i) multiplied with all input values (x_i):

$$\boldsymbol{u} = \sum_{i=1}^{n} \boldsymbol{x_i w_i}. \tag{2}$$

In the case of first hidden layer, input values are image pixels values. In this research three basic activation functions are used, and these functions are: Tanh, Logistic sigmoid and ReLU [36 – 38].

2.2.1 Tanh Activation Function

Tanh activation function is, in fact, a hyperbolic tangent function [36] and it can be written as:

$$\boldsymbol{f(x) = tanh(x) = \frac{(e^x - e^{-x})}{(e^x + e^{-x})}}, \tag{3}$$

where x represents function argument, in case of AN argument is result of the sum, u. This functions maps values from domain interval:

$$-\infty < x < \infty, \tag{4}$$

into the codomain interval

$$-\mathbf{1} < f(x) < 1. \tag{5}$$

2.2.2 Logistic Sigmoid Activation Function

Logistic sigmoid activation function can be written as [39]:

$$\boldsymbol{f(x) = \frac{1}{(1 + e^{-x})}}. \tag{6}$$

A key difference between Logistic sigmoid and Tanh activation function is that Logistic sigmoid maps all domain values into the co-domain interval:

$$\mathbf{0} < f(x) < 1. \tag{7}$$

In the case when Logistic sigmoid is used, output value will be positive. This does not have to be a case when Tanh activation function is used.

2.2.3 ReLU Activation Function

As a difference of aforementioned activation functions, ReLU activation function does not transform input values [40]. In the case of ReLU activation function, output values will be equal to input values if input values are greater than zero. This property can be written as:

$$\boldsymbol{f(x)} = \begin{cases} \mathbf{0}, & x < 0 \\ \boldsymbol{x}, & x \geq 0 \end{cases}. \tag{8}$$

By combining ANs, MLP can be constructed [41]. Block scheme of used MLP is shown in Fig. 3. In the block scheme of MLP, each circle represents one AN together with sum

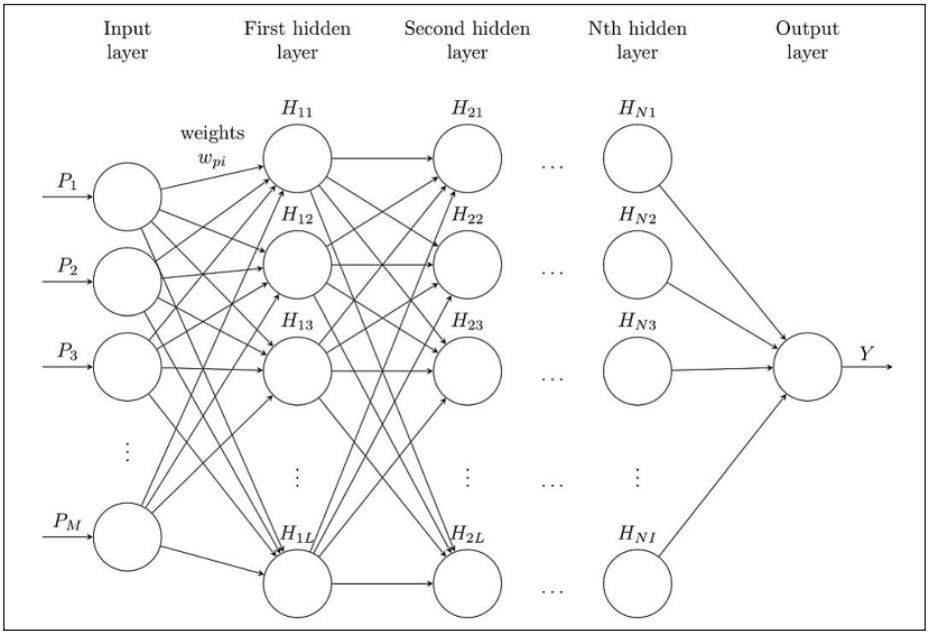

Fig. 3 Block scheme of used MLP

Source: Authors

Table 2 Configurations of hidden layers with number of neurons in each layer

	Hidden layers			
No.	**1**	**2**	**3**	**4**
1.	50	-	-	-
2.	100	-	-	-
3.	50	20	-	-
4.	100	20	-	-
5.	100	50	20	-
6.	100	50	50	20

Source: Authors

and activation function. Input nodes are shown at the left side of the block scheme and the output node is shown at the right side. Lines between nodes are representing synapses between neurons.

In order to find relations between input and output values of the described dataset, technique called supervised learning is used. Supervised learning is the machine learning technique that maps input values to paired output value. This is achieved by using optimization algorithms (solvers). In the case of this research, three different solvers are utilized, and these are:

- Limited-memory Broyden-Fletcher-Goldfarb-Shanno algorithm (L-BFGS) [42],
- Stochastic gradient descent algorithm (SGD) [43] and
- Adaptive learning rate optimization algorithm (Adam) [44].

In this research, six different configurations of MLP hidden layers are designed. All configurations are shown in Table 2, where first column represents numerical designation of each configuration. In other columns (2-5), number of neurons is shown for each hidden layer respectively. On this way, six different configurations of MLP are designed.

3 Research methodology

For the analysis performed in this paper, 54 different MLPs are designed by varying different activation functions, solvers and configurations of hidden layers. On this way, aforementioned MLPs are trained and tested for each of decay state coefficients individually. As a first measure of MLP regression performance, mean relative error of each predicted decay state coefficient is used. Mean relative error can be calculated as:

$$\overline{\boldsymbol{d}} = \frac{\mathbf{1}}{\boldsymbol{N}}\sum_{\boldsymbol{i}=\mathbf{1}}^{\boldsymbol{N}} \boldsymbol{d_i}, \tag{9}$$

where N is the number of samples in test dataset and d_i is a percent relative error of predicted decay state coefficient, calculated as:

$$\boldsymbol{d_i} = \frac{|\boldsymbol{y_{ti}} - \boldsymbol{y_{ri}}|}{\boldsymbol{y_{ti}}} \cdot \mathbf{100}\,, \tag{10}$$

where y_{ti} represents true value of decay state coefficient and y_{ri} represents predicted decay state coefficient for one sample of input parameters. By using Eq. (9) and Eq. (10), mean relative error of each MLP will be calculated. In the case of both decay state coefficients, MLP with the lowest mean relative error for each activation function will be presented. For aforementioned MLPs, mean relative error for each value of decay state coefficient in test dataset will be calculated as:

$$\overline{\boldsymbol{d_p}} = \frac{\mathbf{1}}{\boldsymbol{M}}\sum_{\boldsymbol{j}=\mathbf{1}}^{\boldsymbol{M}} \boldsymbol{d_j}, \tag{11}$$

where M represents number of samples with the same value of true decay state coefficient, and d_j is calculated as:

$$\boldsymbol{d_j} = \frac{\boldsymbol{y_{tj}} - \boldsymbol{y_{rj}}}{\boldsymbol{y_{tj}}} \cdot \mathbf{100}\,. \tag{12}$$

By using presented criteria, possibility of MLP utilization for prediction of GT compressor decay state coefficient and GT decay state coefficient will be discussed.

4 Results and discussion

4.1 Prediction of GT compressor decay state coefficient

When MLPs for prediction of GT compressor decay state coefficient are compared, it can be seen that mean relative error lower than 1.3 % is achieved if Logistic sigmoid or Tanh activation function is used, as shown in Table 3. In the case of Logistic sigmoid activation function, the lowest mean relative error achieved is 1.094 %. A slightly higher mean relative error of 1.294 % is achieved if Tanh activation function is utilized. If MLPs are designed with ReLU activation function, error rates are significantly higher. The lowest mean relative error achieved with these MLPs is 11.421 %. It can be noticed that the lowest mean relative error of MLP designed with any of three afore-

Table 3 MLP configurations with the lowest mean relative error for each activation function (GT compressor decay state coefficient)

Activation function	Logistic sigmoid	ReLU	Tanh
Configuration of hidden layers	2.	6.	1.
Solver	L-BFGS	L-BFGS	L-BFGS
Mean error [%]	1.094	11.421	1.294

Source: Authors

mentioned activation functions is achieved if L-BFGS solver is utilized.

If Logistic sigmoid activation function is used, MLP achieves the highest accuracy if it is designed with one hidden layer of 100 ANs. In the case of Tanh, the lowest mean relative error is achieved if MLP with one hidden layer of 50 Ans is utilized. In the case of ReLU activation function, the lowest mean relative error is achieved if MLP is designed with four hidden layers with 100, 50, 50 and 20 ANs, respectively.

When mean relative errors for each of real values in test dataset are compared it can be seen that, if ReLU activation function is used, the highest mean relative error occurs in the case when the real value is equal to 0.965. In all other cases, mean relative error is, in the absolute value, lower than 25 %, as shown in Fig. 4.

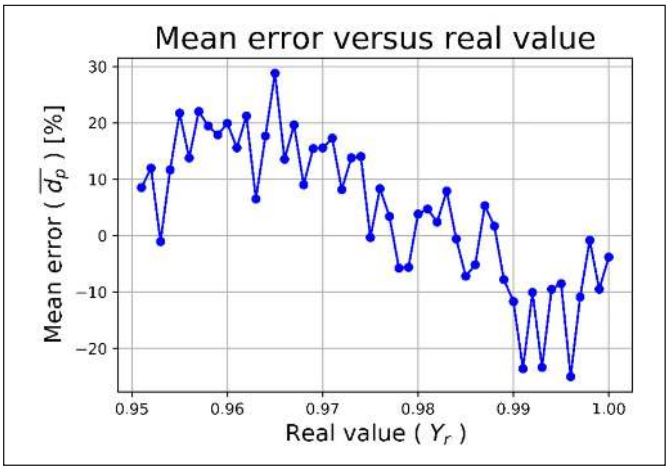

Fig. 4 Mean relative error of GT compressor decay state coefficient prediction for each real value in the case of ReLU activation function

Source: Authors

In the case of Tanh activation function, it can be noticed that mean relative error, in absolute value, do not exceed 3 %, regardless of the real value. It can also be noticed that the lowest mean relative error is achieved for samples with real value between 0.97 and 0.98, as shown in Fig. 5.

Furthermore, in Fig. 5 can be noticed that for samples with lower real value, predicted values are higher than real, while in the case of higher real values, values predicted with MLP are slightly lower.

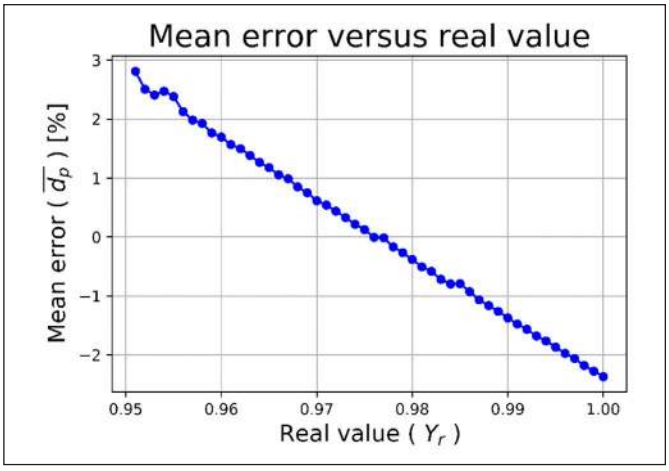

Fig. 5 Mean relative error of GT compressor decay state coefficient prediction for each real value in the case of Tanh activation function

Source: Authors

Similar properties are noticed in the case of Logistic sigmoid activation function, Fig. 6. In this case, MLP also achieves mean absolute value of relative errors lower than 3 %. Most significant difference between two aforementioned MLPs is slightly higher oscillations of mean error values in the case of Logistic sigmoid activation function. Described trend in regard of positive and negative relative errors is also present, as shown in Fig. 6.

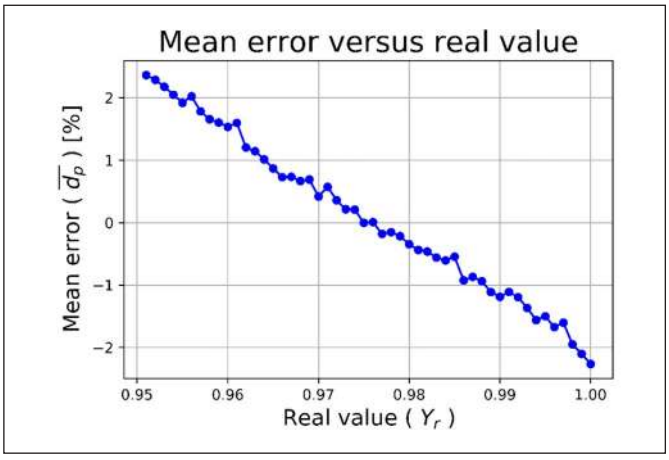

Fig. 6 Mean relative error of GT compressor decay state coefficient prediction for each real value in the case of Logistic sigmoid activation function

Source: Authors

Table 4 MLP configurations with the lowest error for each activation function (GT decay state mean relative coefficient)

Activation function	Logistic sigmoid	ReLU	Tanh
Configuration of hidden layers	6.	4.	1.
Solver	L-BFGS	Adam	L-BFGS
Mean error [%]	0.635	21.124	0.622

Source: Authors

4.2 Prediction of GT decay state coefficient

When mean relative errors of MLPs for GT decay state coefficient prediction are compared it can be seen that similar error rates are achieved if Logistic sigmoid and Tanh activation functions are used. MLP designed with Logistic sigmoid activation function achieves mean relative error of 0.635 %, while MLP designed with Tanh activation function achieves mean relative error of 0.622 %. In both cases L-BFGS solver is utilized during MLP training. MLP designed with Logistic sigmoid activation function achieves minimal mean relative error if configuration of hidden layers No. 6 (Table 2) is utilized. That is not a case if Tanh activation function is used. This MLP achieves the lowest mean relative error if configuration with one hidden layer of 50 ANs is utilized. MLP designed with ReLU activation function achieves minimal mean relative error of 21.124 % if configuration with one hidden layer of 100 and one hidden layer of 20 ANs is utilized, as shown in Table 4.

When MLP GT decay state coefficient prediction is performed by using ReLU activation function, it can be noticed that the highest errors are achieved in cases of the lower coefficient real values. The lowest errors are achieved for GT decay state coefficients between the values of 0.988 and 0.989. If this MLP is utilized for higher GT decay state coefficient values, it can be noticed that the relative errors, in absolute value, are notably high. It can also be noticed that the relative errors achieved on lower real values of GT decay state coefficient are positive, while those achieved on higher real values of GT decay state coefficient are negative, Fig. 7.

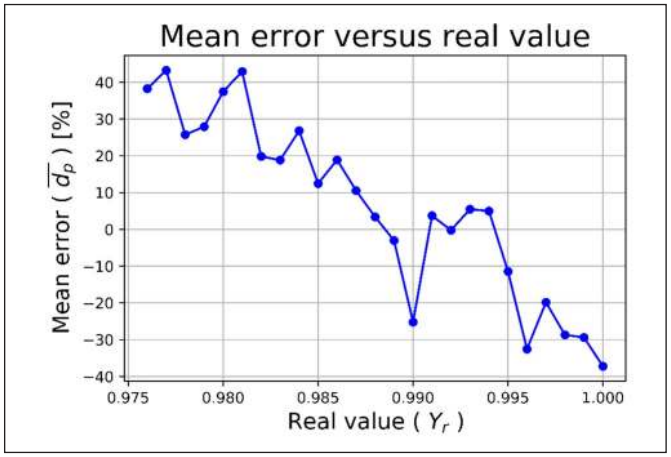

Fig. 7 Mean relative error of GT decay state coefficient prediction for each real value in the case of ReLU activation function

Source: Authors

In the case of MLP designed with Tanh activation function, it can be seen that the lowest mean relative errors are achieved for prediction of GT decay state coefficient with real values between 0.985 and 0.990. Such MLP, in average, achieves higher values in case of lower GT decay state coefficient values and lower values for higher GT decay state coefficient values, as shown in Fig. 8. The described trend is similar to previously shown cases.

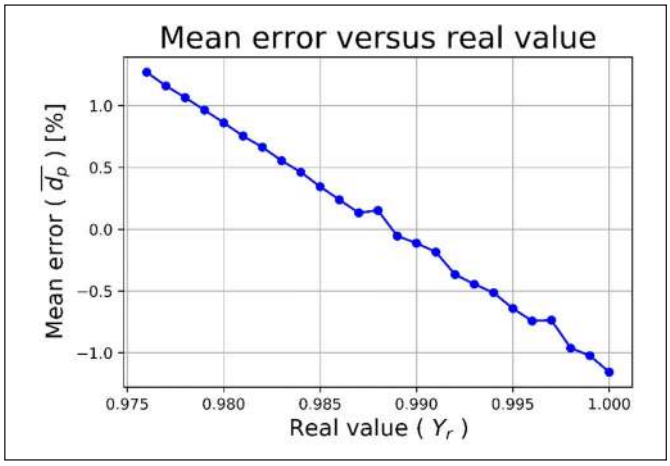

Fig. 8 Mean relative error of GT decay state coefficient prediction for each real value in the case of Tanh activation function

Source: Authors

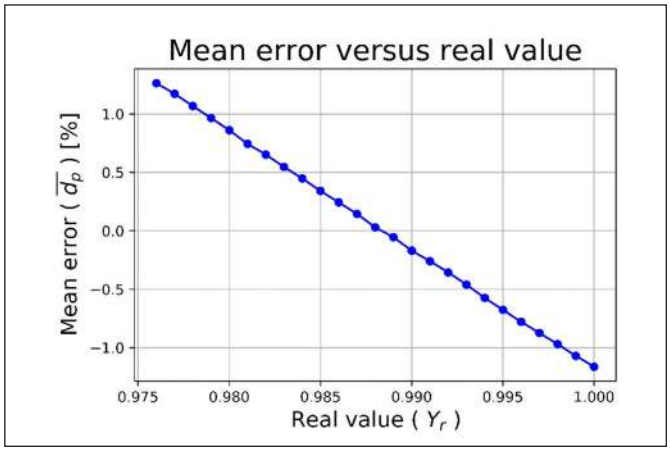

Fig. 9 Mean relative error of GT decay state coefficient prediction for each real value in the case of Logistic sigmoid activation function

Source: Authors

Similar results are achieved if Logistic sigmoid activation function is used. In this case, the lowest mean relative error is achieved for prediction of the GT decay state coefficient with the true value of 0.988. As in the case shown in Fig. 8, MLP achieves slightly higher values for prediction of lower GT decay state coefficient values and slightly lower values for prediction of higher GT decay state coefficient values as shown in Fig. 9.

When all presented results are summarized, it can be concluded that MLPs designed with Tanh and Logistic sigmoid activation function are performing with lower error rate, in comparison to MLPs designed with ReLU activation function. This property occurs for prediction of both decay state coefficients. In the case of GT decay state coefficient prediction, lower mean relative errors are achieved in comparison to the case of GT compressor decay state coefficient prediction. In the case of GT decay state coefficient prediction, the lowest achieved mean relative error is 0.622 %, while in the case of GT compressor decay state coefficient prediction, the lowest achieved mean relative error is 1.094 %, as shown in Fig. 10.

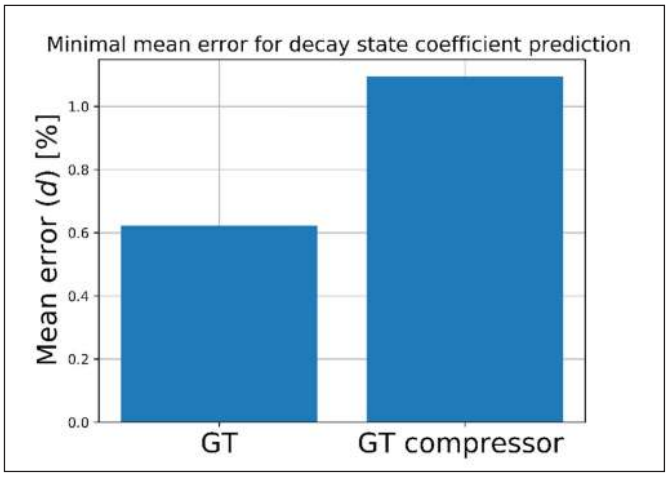

Fig. 10 Comparison of minimal mean errors of GT and GT compressor decay state coefficient prediction

Source: Authors

5 Conclusion

In this paper, an MLP approach to condition-based maintenance of CODLAG propulsion system vital components (GT and GT compressor) is presented. Influence of MLP hyperparameters on prediction error is observed and mean error for each configuration is presented. After that, mean prediction error for each true value of decay state coefficient is calculated (for both GT and GT compressor), and results are compared. From presented results, the following conclusions can be drawn:

- There is a possibility for MLP implementation in solving tasks of condition-based maintenance of CODLAG propulsion system and in tasks of GT and GT compressor decay state coefficients prediction,
- The lowest error rates are achieved if Tanh or Logistic sigmoid activation functions are used for MLP design, while MLPs designed with ReLU activation function are performing with higher prediction error,
- The lowest error rates are achieved if L-BFGS solver is used for MLP training.

Based on presented results, it can be concluded that in future studies, a similar approach can be used for condition-based maintenance of other marine propulsion systems, such as diesel engines and steam turbines.

Acknowledgment

This research has been (partly) supported by the CEEPUS network CIII-HR-0108, European Regional Development Fund under the grant KK.01.1.1.01.0009 (DATACROSS) and University of Rijeka scientific grant uniri-tehnic-18-275-1447.

References

[1] Ahmad, R., & Kamaruddin, S. (2012). An overview of time-based and condition-based maintenance in industrial application. Computers & Industrial Engineering, 63(1), 135-149. (doi:10.1016/j.cie.2012.02.002)

[2] Yam, R. C. M., Tse, P. W., Li, L., & Tu, P. (2001). Intelligent predictive decision support system for condition-based maintenance. The International Journal of Advanced Manufacturing Technology, 17(5), 383-391. (doi:10.1007/s001700170173)

[3] Grall, A., Bérenguer, C., & Dieulle, L. (2002). A condition-based maintenance policy for stochastically deteriorating systems. Reliability Engineering & System Safety, 76(2), 167-180. (doi:10.1016/s0951-8320(01)00148-x)

[4] Li, Y. G., & Nilkitsaranont, P. (2009). Gas turbine performance prognostic for condition-based maintenance. Applied energy, 86(10), 2152-2161. (doi:10.1016/j.apenergy.2009.02.011)

[5] Jardine, A. K., Lin, D., & Banjevic, D. (2006). A review on machinery diagnostics and prognostics implementing condition-based maintenance. Mechanical systems and signal processing, 20(7), 1483-1510. (doi:10.1016/j.ymssp.2005.09.012)

[6] Coraddu, A., Oneto, L., Ghio, A., Savio, S., Anguita, D., & Figari, M. (2016). Machine learning approaches for improving condition-based maintenance of naval propulsion plants. Proceedings of the Institution of Mechanical Engineers, Part M: Journal of Engineering for the Maritime Environment, 230(1), 136-153. (doi:10.1177/1475090214540874)

[7] Cipollini, F., Oneto, L., Coraddu, A., Murphy, A. J., & Anguita, D. (2018). Condition-based maintenance of naval propulsion systems with supervised data analysis. Ocean Engineering, 149, 268-278. (doi:10.1016/j.oceaneng.2017.12.002)

[8] Coraddu, A., Oneto, L., Ghio, A., Savio, S., Figari, M., & Anguita, D. (2015, March). Machine learning for wear forecasting of naval assets for condition-based maintenance applications. In 2015 International Conference on Electrical Sys-

tems for Aircraft, Railway, Ship Propulsion and Road Vehicles (ESARS) (pp. 1-5). IEEE. (doi:10.1109/esars.2015.7101499)

[9] Mrzljak, V., Medica, V., Bukovac, O.: Simulation of a Two-Stroke Slow Speed Diesel Engine Using a Quasi-Dimensional Model, Transactions of Famena 2, p. 35-44, 2016. (https://doi.org/10.21278/TOF.40203)

[10] Feng, Y., Wang, H., Gao, R., Zhu, Y.: A Zero-Dimensional Mixing Controlled Combustion Model for Real Time Performance Simulation of Marine Two-Stroke Diesel Engines, Energies 12 (10), 2000, 2019. (https://doi.org/10.3390/en12102000)

[11] Mrzljak, V., Medica, V., Bukovac, O.: Volume agglomeration process in quasi-dimensional direct injection diesel engine numerical model, Energy 115, p. 658-667, 2016. (https://doi.org/10.1016/j.energy.2016.09.055)

[12] Wang, G., Yu, W., Li, X., Su, Y., Yang, R., Wu, W.: Experimental and numerical study on the influence of intake swirl on fuel spray and in-cylinder combustion characteristics on large bore diesel engine, Fuel 237, p. 209–221, 2019. (https://doi.org/10.1016/j.fuel.2018.09.156)

[13] Wang, Z., Kuang, H., Zhang, J., Chu, L., Ji, Y.: Nitrogen Oxide Removal by Coal-Based Activated Carbon for a Marine Diesel Engine, Applied sciences 9 (8), 1656, 2019. (https://doi.org/10.3390/app9081656)

[14] Senčić, T., Mrzljak, V., Blecich, P., Bonefačić, I.: 2D CFD Simulation of Water Injection Strategies in a Large Marine Engine, Journal of Marine Science and Engineering 7 (9), 296, 2019. (https://doi.org/10.3390/jmse7090296)

[15] Koroglu, T., Sogut, O. S.: Conventional and Advanced Exergy Analyses of a Marine Steam Power Plant, Energy 163, p. 392-403, 2018. (https://doi.org/10.1016/j.energy.2018.08.119)

[16] Mrzljak, V., Poljak, I., Mrakovčić, T.: Energy and exergy analysis of the turbo-generators and steam turbine for the main feed water pump drive on LNG carrier, Energy Conversion and Management, 140, p. 307–323, 2017. (https://doi.org/10.1016/j.enconman.2017.03.007)

[17] Mrzljak, V., Poljak, I., Prpić-Oršić, J.: Exergy analysis of the main propulsion steam turbine from marine propulsion plant, Shipbuilding: Theory and Practice of Naval Architecture, Marine Engineering and Ocean Engineering 70 (1), p. 59-77, 2019. (http://dx.doi.org/10.21278/brod70105)

[18] Mrzljak, V., Senčić, T., Žarković, B.: Turbogenerator Steam Turbine Variation in Developed Power: Analysis of Exergy Efficiency and Exergy Destruction Change, Modelling and Simulation in Engineering 2018. (https://doi.org/10.1155/2018/2945325)

[19] Lorencin, I., Anđelić, N., Mrzljak, V., Car, Z.: Exergy analysis of marine steam turbine labyrinth (gland) seals, Pomorstvo: scientific journal of maritime research, 33 (1), p. 76-83, 2019. (https://doi.org/10.31217/p.33.1.8)

[20] Marques, C. H., Caprace, J.-D., Belchior, C. R. P., Martini, A.: An Approach for Predicting the Specific Fuel Consumption of Dual-Fuel Two-Stroke Marine Engines, Journal of Marine Science and Engineering 7 (2), 20, 2019. (https://doi.org/10.3390/jmse7020020)

[21] Fernández, I. A., Gómez, M. R., Gómez, J. R., Insua, A. A. B.: Review of propulsion systems on LNG carriers, Renewable and Sustainable Energy Reviews 67, p. 1395–1411, 2017. (https://doi.org/10.1016/j.rser.2016.09.095)

[22] Ammar, N. R.: Environmental and cost-effectiveness comparison of dual fuel propulsion options for emissions reduction onboard LNG carriers, Shipbuilding: Theory and Practice of Naval Architecture, Marine Engineering and Ocean Engineering 70 (3), p. 61-77, 2019. (http://dx.doi.org/10.21278/brod70304)

[23] Ammar, N. R., Seddiek, I. S.: Eco-environmental analysis of ship emission control methods: Case study RO-RO cargo vessel, Ocean Engineering 137, p. 166–173, 2017. (https://doi.org/10.1016/j.oceaneng.2017.03.052)

[24] Bourlard, H., & Kamp, Y. (1988). Auto-association by multilayer perceptrons and singular value decomposition. Biological cybernetics, 59(4-5), 291-294. (doi:10.1007/bf00332918)

[25] Bogović, K., Lorencin, I., Anđelić, N., Blažević, S., Smolčić, K., Španjol, J., Car, Z. (2018, January). Artificial Intelligence-Based Method for Urinary Bladder Cancer Diagnostic. In International Conference on Innovative Technologies, IN-TECH 2018.

[26] Lorencin, I., Barišić B., Anđelić, N., Španjol, J., Car, Z. (2019, January). Comparison of Edge Detectors for Urinary Bladder Cancer Diagnostic. In International Conference on Innovative Technologies, IN-TECH 2019.

[27] Brnić, M., Čondrić, E., Blažević, S., Anđelić, N., Borović, E., & Car, Z. (2018, January). Sepsis Prediction Using Artificial Intelligence Algorithms. In International Conference on Innovative Technologies, IN-TECH 2018.

[28] Lorencin, I., Anđelić, N., Mrzljak, V., Car, Z. (2019). Marine Objects Recognition Using Convolutional Neural Networks NAŠE MORE: znanstveno-stručni časopis za more i pomorstvo, 66(3), (doi: 10.17818/NM/2019/3.2)

[29] Bukovac, O., Medica, V., & Mrzljak, V. (2015). Steady state performances analysis of modern marine two-stroke low speed diesel engine using MLP neural network model. Shipbuilding: Theory and Practice of Naval Architecture, Marine Engineering and Ocean Engineering 66(4), 57-70.

[30] Yawen Li, Guangcan Tang, Jiameng Du, Nan Zhou, Yue Zhao, and Tian Wu. Multilayer perceptron method to estimate real-world fuel consumption rate of light duty vehicles. IEEE Access, 7:63395–63402, 2019.

[31] Matheus B Moura, Daniel C Vidal, Carla Schueler, Leni J de Matos, and Tadeu N Ferreira. Outdoor-to-indoor power prediction for 768 mhz wireless mobile transmission using multilayer perceptron. In 2018 International Joint Conference on Neural Networks (IJCNN), pages 1–7. IEEE, 2018.

[32] Mat Nizam Mahmud, Mohammad Nizam Ibrahim, Muhammad Khusairi Osman, and Zakaria Hussain. A robust transmission line fault classification scheme using class-dependent feature and 2-tier multilayer perceptron network. Electrical Engineering, 100(2):607–623, 2018.

[33] Thamil Alagan Muthusamy and Neela Ramanathan. An expert system based on least mean square and neural network for classification of power system disturbances. 2018.

[34] Kostyuk, A., Frolov, V.: Steam and gas turbines, Mir Publishers, Moscow, 1988.

[35] Schmidhuber, J. (2015). Deep learning in neural networks: An overview. Neural networks, 61, 85-117. (https://doi.org/10.1016/j.neunet.2014.09.003)

[36] Karlik, B., & Olgac, A. V. (2011). Performance analysis of various activation functions in generalized MLP architectures of neural networks. International Journal of Artificial Intelligence and Expert Systems, 1(4), 111-122.

[37] Zadeh, M. R., Amin, S., Khalili, D., & Singh, V. P. (2010). Daily outflow prediction by multi layer perceptron with logistic

sigmoid and tangent sigmoid activation functions. Water resources management, 24(11), 2673-2688. (https://doi.org/10.1007/s11269-009-9573-4)

[38] Maas, A. L., Hannun, A. Y., & Ng, A. Y. (2013, June). Rectifier nonlinearities improve neural network acoustic models. In Proc. icml (Vol. 30, No. 1, p. 3).

[39] Xu, B., Huang, R., & Li, M. (2016). Revise saturated activation functions. arXiv preprint arXiv:1602.05980.

[40] Li, Y., & Yuan, Y. (2017). Convergence analysis of two-layer neural networks with relu activation. In Advances in Neural Information Processing Systems (pp. 597-607).

[41] Alghoul, A., Al Ajrami, S., Al Jarousha, G., Harb, G., & Abu-Naser, S. S. (2018). Email Classification Using Artificial Neural Network.

[42] Ciyou Zhu, Richard H Byrd, Peihuang Lu, and Jorge Nocedal. Algorithm 778: Lbfgs-b: Fortran subroutines for large-scale bound-constrained optimization. ACM Transactions on Mathematical Software (TOMS), 23(4):550–560, 1997.

[43] Léon Bottou. Large-scale machine learning with stochastic gradient descent. In Proceedings of COMPSTAT'2010, pages 177–186. Springer, 2010. (doi:10.1007/978-3-7908-2604-3_16)

[44] Diederik P Kingma and Jimmy Ba. Adam: A method for stochastic optimization. arXiv preprint arXiv:1412.6980, 2014.